Proceedings of ASME Turbo Expo 2011
GT2011
June 6-10, 2011, Vancouver, British Columbia, Canada

GT2011-46844

A METHOD TO OBTAIN PLANAR MIXTURE FRACTION STATISTICS IN TURBULENT FLOWS SEEDED WITH TRACER PARTICLES

M. Pernpeintner, M. Lauer, C. Hirsch*, T. Sattelmayer
Lehrstuhl für Thermodynamik, TU München
85748, Garching, Germany
E-mail: hirsch@td.mw.tum.de

ABSTRACT
We present a new method to obtain the mixture fraction probability density functions (PDF) of turbulent mixing in planar sections of a flow field which is seeded with PIV tracer particles. We derive a model how the observed scattered light obtained locally in a laser light sheet results from the local mixture fraction PDF and the particle density PDF. From this model we develop an analytical as well as a numerical inversion procedure that allows the deconvolution of the mixture fraction PDF from the light intensity PDF using the measured seeding PDF. We explain the experimental procedure necessary to apply the new technique on the example of a turbulent free jet. The results of both the analytical and the numerical method are compared and the method is then validated against the literature data. Since the method seems applicable whenever PIV measurements can be made it bears high potential for combustor development as it allows to obtain mixing statistics using basically the same measurement hardware.

NOMENCLATURE
Symbols

$\tilde{\Theta}$	intensity [counts]
$\tilde{\omega}$	particle number density $[1/m^3]$
Θ	normalized intensity $[-]$
ω	normalized particle density [-]
f	mixture fraction $[\frac{\mathrm{kg}}{\mathrm{kg_{tot}}}]$
$p_y(x)$	PDF of y to argument x $[-]$
e^x	Exponential function to argument x $[-]$
$\ln x$	natural logarithm function to argument x $[-]$
$F(a)$	Fourier transform of function a
$F^{-1}(a)$	inverse Fourier transform of function a
$M_{k,j}$	linear equation matrix $[-]$
$\delta_{k,j}$	Kronecker delta ($=1$ for $k=j$, else 0) $[-]$
$\delta(x)$	Dirac delta ($=\infty$ for $x=0$, else 0) $[-]$
r	radial coordinate [m]
x	axial coordinate [m]
d	nozzle diameter [m]
U	mean velocity [m/s]
Φ	transported quantity ($=U, f, T..$) in eqn. 16
ρ	density $[\mathrm{kg/m^3}]$
ν	kinematic viscosity $[\mathrm{m^2/s}]$

Indices and Abbreviations

c	jet axis value
PDF	probability density function
PIV	particle image velocimetry
j,k,m	indices of matrix or PDF bin
eff	effective diameter, jet density
TiO_2	titanium dioxide
Re	Reynoldsnumber (eqn. 16)
St	Stokesnumber

INTRODUCTION
In combustor development the statistics of flow turbulence and of mixture fraction are important quantities. While with Particle Image Velocimetry (PIV) the determination of flow statistics even in reacting flows has become a standard and fairly inexpensive experimental tool the measurement of mixture statistics is still a difficult and usually very expensive task. When intrusive

*Address all correspondence to this author.

suction probe measurements with gas analysis and elementary balances are used to map the mixture fraction distribution in a combustor long and costly measurement campaigns are needed. Also the response time of the sampling system and the gas analyzer will typically not allow the resolution of fluctuations. Non-intrusive spectroscopic laser techniques like Rayleigh and Raman scattering [1,2] have been developed which can provide this data. But the particular experimental experience needed, the required hardware and the post-processing software do not make them available for standard design loop investigations. Laser induced fluorescence with tracer substances like acetone [3] is often used in low temperature mixing investigations, e.g. in reciprocating engine applications where either temperatures are low or residence time is short. In gas turbine combustors these conditions are typically not met. Here mixing investigations based on inert tracer particles scattering light which are frequently used in PIV could close a diagnostic gap.

Turbulent mixing studies based on tracer particles have a long tradition [4–7]. The technique is based on seeding only one of the mixing flows with tracer particles while illuminating the measurement volume in the mixing region with a strong light source. As the particles scatter light proportional to their number density the scattered light intensity is proportional to the amount of fluid from the seeded flow in the measurement volume and is thus a measure of mixing. In this technique the particles must be small enough to follow the fluid and must be large in number as to provide a quasi-continuum in which the light scattering intensity depends mainly on the local particle density. Typically local intensity measurements are made in the mixing field and at a fixed reference location where the seeded flow is entirely unmixed. With constant homogeneous seeding and constant light source the intensity from the mixing field can be normalized with the reference intensity. In the constant density case this is a direct measure of mixture fraction, whereas in varying density it can be related to mixture fraction through a constitutive relation [7]. If the seeding is not constant or the light source is fluctuating the momentary reference intensity must be measured simultaneously with the mixing field intensity to compensate the fluctuations. While this will take care of the fluctuations of the light source since these are seen instantaneously in both places it can compensate fluctuations of the seeding quality only if the frequency of seeding fluctuation is very low or convection time between reference and measurement location is very short. Only in this case it can be assumed that both reference and measurement volume see the same seeding density. Sautet and Stepowski [7] report that otherwise the seeding fluctuations will overlay on the desired fluctuations of mixing and distort the result.

In this paper we present a new statistical method to obtain the mixture fraction probability density functions (PDF) of turbulent mixing in planar sections of a flow field which is seeded with PIV tracer particles. We found that the Mie scattering images display locally a convolution of the desired mixing statistic with the seeding particle density statistic. Our statistical approach allows us, based on this relation, to gain the desired mixture fraction PDF from the scattering image series. Compared to previous techniques, the proposed method has a decisive advantage: as we will show below, fluctuations of laser power, seeding density and particle size are automatically considered and do not influence the results within a certain range. Furthermore, the discrete nature of the seeding particles is taken into account, which would otherwise contribute to the variance of the measured light intensity and overlay the variance of the mixture fraction.

In the theory part we show how the observed scattered light statistic obtained locally in a laser light sheet results from the local mixture fraction PDF and the particle density PDF. From this model we develop an analytical as well as a numerical inversion procedure that allows the deconvolution of the mixture fraction PDF from the light intensity PDF using the seeding PDF which is the scattered light PDF measured at the reference location. Then we explain the detailed experimental procedure necessary to apply the new technique on the example of a turbulent free jet. The results of both the analytical and the numerical method are compared and the method is validated against the literature data.

THEORY

In this section we derive a statistical model of the particle scattering process to connect the probability density function of the normalized light intensity $p_\Theta(\Theta)$ with those of the normalized particle density $p_\omega(\omega)$ and the mixture fraction $p_f(f)$. Then we show two methods that can be used to deconvolve the desired statistics of mixture fraction from that of the measured light intensity.

Normalized variables, seeding density PDF

As the scattering light technique is based on relative intensities we consider normalized variables. We introduce the normalized light intensity

$$\Theta = \frac{\tilde{\Theta}}{\tilde{\Theta}_0} \quad \text{and} \quad 0 \leq \Theta \leq 1 \tag{1}$$

and the normalized particle density

$$\omega = \frac{\tilde{\omega}}{\tilde{\omega}_0} \quad \text{and} \quad 0 \leq \omega \leq 1. \tag{2}$$

Following e.g. Sautet and Stepowski [7] the reference values $\tilde{\omega}_0$ and $\tilde{\Theta}_0$ are defined at the entrance of the seeded fluid into the mixing zone where $f = 1$ and $p_f(f) = \delta(f-1)$. In this case the probability density function of the normalized light intensity and that of the normalized particle density are identical:

$$p_\Theta(\Theta) = p_\omega(\omega) \quad \text{for} \quad f = 1. \tag{3}$$

This means that the PDF of the seeding density is the measured scattered light PDF at the entrance of the seeded flow into the mixing zone. This scattered light intensity also contains the fluctuations of laser power.

PDF of scattered light

We now derive a model for the PDF of the observed scattered light Θ as a function of mixture fraction f and particle density ω. For this we make two assumptions.

1. Seeding density ω and mixture fraction f are statistically independent and have the probability density functions $p_\omega(\omega)$ and $p_f(f)$.
2. The local momentary intensity is given by:

$$\Theta = \omega \cdot f \tag{4}$$

The first assumption is plausible in the turbulent convective mixing regime, where the seeding particles will follow the seeded fluid and preserve their particle distribution [8]. Therefore, while there will be a distribution of particle density (or even particle size), this will not be influenced by the mixing process.

The second assumption considers that the seeding particles are much smaller than the turbulence sizes and sufficient in number such that they can be treated as a quasi-continuum [8].

We now consider a volume in the mixing flow small enough that we can assume constant values for seeding density ω and mixture fraction f. The probability that $\omega \in [\omega_1; \omega_1 + d\omega]$ is given by $p_\omega(\omega_1)\,d\omega$. In analogy we have for the mixture fraction $f \in [f_1; f_1 + df]$ the probability $p_f(f_1)\,df$. Invoking statistical independence the probability of meeting both conditions $\omega \in [\omega_1; \omega_1 + d\omega]$ and $f \in [f_1; f_1 + df]$ is the product $p_\omega(\omega_1)\,d\omega \cdot p_f(f_1)\,df$. The measured intensity is in this case $\Theta = \omega_1 \cdot f_1$. As $0 \leq \omega_1 \leq 1$ and $0 \leq f_1 \leq 1$, different combinations of ω_1 and f_1 may give the same Θ, so we must integrate over all values with the condition $\delta(\Theta - \omega_1 \cdot f_1)$ to obtain the probability density of Θ.

$$p_\Theta(\Theta) = \int_0^1 \int_0^1 p_\omega(\omega_1) \cdot p_f(f_1) \cdot \delta(\Theta - \omega_1 \cdot f_1)\, d\omega_1\, df_1 \tag{5}$$

Dropping indices for ease of notation and using the substitution $\delta(\Theta - \omega \cdot f) = \frac{1}{\omega}\delta\left(f - \frac{\Theta}{\omega}\right)$ allows the integration over f giving the desired model equation.

$$p_\Theta(\Theta) = \int_0^1 p_\omega(\omega) \cdot \frac{1}{\omega} \cdot p_f\left(\frac{\Theta}{\omega}\right) d\omega \tag{6}$$

Analytical inversion

For an analytical inversion of eqn. 6 we introduce the following transformations: $\hat{f} = \ln f$, $\hat{\omega} = \ln \omega$, $\hat{\Theta} = \ln \Theta$. Recognizing that $d\omega = \omega\, d\hat{\omega}$, eqn. 6 is written:

$$p_\Theta\left(e^{\hat{\Theta}}\right) = \int_{-\infty}^0 p_\omega\left(e^{\hat{\omega}}\right) \cdot p_f\left(e^{\hat{\Theta}-\hat{\omega}}\right) d\hat{\omega} \tag{7}$$

Substituting $\hat{p}_k(k) = p_k(e^k)$ for all three variables $k = \Theta, \omega, f$ eqn. 7 becomes a convolution integral.

$$\hat{p}_\Theta\left(\hat{\Theta}\right) = \int_{-\infty}^0 \hat{p}_\omega\left(\hat{\omega}\right) \cdot \hat{p}_f\left(\hat{\Theta} - \hat{\omega}\right) d\hat{\omega} \tag{8}$$

Applying the convolution theorem of Fourier transformation, this can be solved as:

$$\hat{p}_f = F^{-1}\left(\frac{F(\hat{p}_\Theta)}{F(\hat{p}_\omega)}\right) \tag{9}$$

which will give the desired result $p_f(f) = \hat{p}_f(\ln f)$. Applying the analytical inversion in practice requires the application of low pass filtering, since the Fourier transform is sensitive to high frequency oscillations. In our investigation we have found the following algorithm to work reasonably well. The measured PDFs p_Θ and p_ω are low pass filtered and then transformed into $\hat{p}_\Theta$ and $\hat{p}_\omega$. From these $\hat{p}_f$ is calculated via Fourier transforms. This is then converted into p_f which is again low pass filtered. The disadvantage is clearly that given steep distributions low pass filtering will broaden these and thus deteriorate in particular the variance of f. However, in some cases with smooth quasi-Gaussian PDFs the method requires no damping and may thus serve as a check for the numerical method outlined below.

Numerical inversion

As eqn. 5 is symmetrical with respect to permutation of the variables f and ω, eqn. 6 is equivalent to:

$$p_\Theta(\Theta) = \int_0^1 p_f(f) \cdot \frac{1}{f} \cdot p_\omega\left(\frac{\Theta}{f}\right) df \tag{10}$$

Since from the digital camera only discrete intensities $\tilde{\Theta}_k$ (with $k = 1..256$) are recorded, all PDFs will be discrete, too. With this in mind eqn. 10 is rewritten as a finite sum.

$$p_\Theta(\Theta_k) = \sum_{j=1}^{256} p_f(f_j) \cdot \frac{1}{f_j} \cdot p_\omega\left(\frac{\Theta_k}{f_j}\right) \cdot \Delta f \tag{11}$$

with $\Theta_k = \frac{k-1/2}{256}$, $f_j = \frac{j-1/2}{256}$, $\Delta f = \frac{1}{256}$ and $k, j = 1...256$.

In eqn. 11 the left side is known and $p_\omega(\Theta_k/f_j)$ can be interpolated from the measured discrete data, so eqn. 11 forms the linear 256x256 equation system

$$M_{k,j} \cdot p_{f,j} = p_{\Theta,k} \tag{12}$$

with $M_{k,j} = (\Delta f / f_j) \cdot p_\omega(\Theta_k/f_j)$. Observing that $p_\omega(\omega > 1) = 0$ the matrix $M_{k,j}$ is an upper triangular form.

While this can principally be solved for the desired PDF of mixture fraction, in practice the system is badly conditioned. We therefore use Tikhonov regularization [9], which results in the following system.

$$\left(M_{m,k} \cdot M_{m,j} - \alpha^2 \cdot \delta_{k,j}\right) p_{f,j} = M_{m,k} p_{\Theta,m} \tag{13}$$

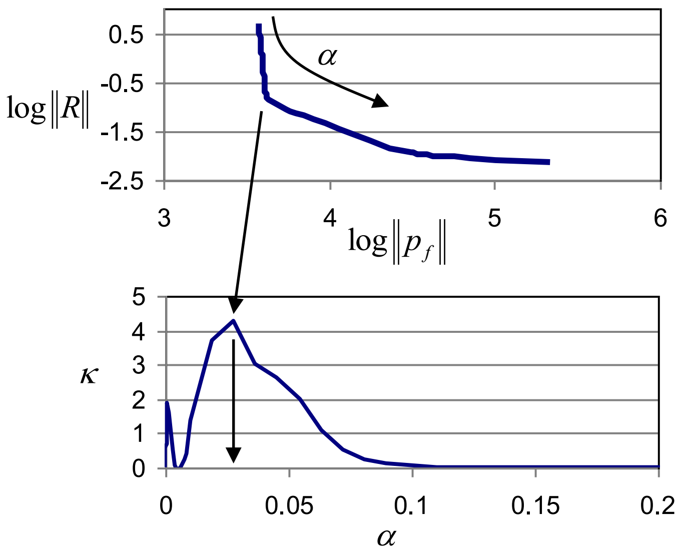

Figure 1. Top: Norm of Residual over norm of solution vector. Bottom: Geometrical curvature of L-curve over stability parameter α.

Here, $\delta_{k,j}$ denotes the Kronecker delta and α is a stability parameter, which controls the condition of the equation system. In most cases α can be chosen on the basis of the L-curve criterion [9]. There eqn. 13 is solved for increasing values of α and the solution $p_{f,j}(\alpha)$ is inserted into the original eqn. 12 calculating the residual norm R of that equation as well as the norm of the solution vector $p_{f,j}(\alpha)$. Plotting this logarithmically results in a typical curve shown on the top in Figure 1. Looking at the curve the optimal choice of α would intuitively be where both the residual as well as the solution vector norm are smallest. This is the location of maximum curvature, which is seen in the bottom graph. There the geometrical curvature of the L-curve is plotted over the values of α. In most cases investigated in this work, this criterion worked well, however, degenerate L-curves exist, where a manual choice of α is necessary. Typical values of α are between 0.02 and 0.07.

Mixture of fluids of different densities

So far, we treated mixture of fluids of equal density. To generalize our results on the case of two non-reacting fluids of different density, eqn. 6 has to be changed slightly. Let ρ_0 be the density of the seeded jet fluid and ρ_∞ the density of the surrounding fluid, according to [7], the local density ρ is a function of the mixture fraction f:

$$\rho = \rho_0 f + \rho_\infty (1-f) \tag{14}$$

Moreover, it is clear that the measured light intensity Θ is proportional to the local density ρ, so that we now have $\Theta = \omega \cdot f \cdot \rho$ instead of $\Theta = \omega \cdot f$. As ρ is a function of f, we can define a new quantity $F = f \cdot \rho$ and write $\Theta = \omega \cdot F$, where ω and F are statistically independent. Analogous to the derivation above (we only have to replace f by F), we obtain

$$p_\Theta(\Theta) = \int_0^1 p_\omega(\omega) \cdot \frac{1}{\omega} \cdot p_F\left(\frac{\Theta}{\omega}\right) d\omega \tag{15}$$

Using the above discussed inversion procedures, we can resolve this equation for p_F. In order to extract p_f from p_F, we use eqn. 14 and the relation $p_F(F)dF = p_f(f)df$, which leeds to

$$\begin{aligned} p_f(f) &= p_F(F)\frac{dF}{df} = p_F(f\rho) \cdot \frac{d(f\rho)}{df} \\ &= p_F(f \cdot (\rho_0 f + \rho_\infty(1-f))) \cdot (2\rho_0 f - 2\rho_\infty f + \rho_\infty) \end{aligned}$$

Classical turbulent jet theory

The classical theory of turbulent round jets describes the behavior of the mean quantities in the self similar range based on the laminar jet solution.

$$\begin{aligned} \frac{\Phi}{\Phi_0} &= \frac{3}{32} \cdot Re \cdot \frac{d}{x} \cdot \left[1 + \frac{\xi^2}{4}\right]^{-2} \\ \xi &= 0.2165 \cdot Re \cdot \frac{r}{x} \\ Re &= \frac{U_0 \cdot d}{\nu} \end{aligned} \tag{16}$$

Here Φ is the transported quantity ($= U, f, T$), d, U_0 are the nozzle diameter and nozzle velocity, r, x are the radial and axial coodinates and ν is the kinematic molecular viscosity. The effect of turbulence is modeled by introducing an effective viscosity $\nu_{\text{eff}} = C \cdot U_0 \cdot d$ in place of the molecular viscosity ν, which is equivalent to fixing the Reynolds number Re to a constant value. These are $Re = 72$ for $\Phi = U$ and $Re = 55$ for $\Phi = f$ to account for the different turbulent transport of momentum and concentration. To account for density differences between the jet fluid and the surrounds in turbulent flow the concept of the effective diameter is used,

$$d_{\text{eff}} = d \cdot \sqrt{\frac{\rho_0}{\rho_\infty}}, \tag{17}$$

which replaces d in eqn. 16. Here again ρ_0 and ρ_∞ are the densities of jet and surrounding fluid.

Influence of particle loading

Though the perception of PIV and Laser Doppler Velocimetry is that of an "non-intrusive" measurement technology the results of our work reported here suggest that this must be considered with care. Though the volume fraction of particles V_p/V_{tot} to reach a high enough particle number density may be small, their mass can already be quite considerable. Seeding an air jet flow with TiO_2-particles the effective jet density can be computed like:

$$\rho_{\mathrm{eff}} = \rho_{\mathrm{air}} \cdot \left(1 - \frac{V_p}{V_{\mathrm{tot}}}\right) + \rho_{\mathrm{TiO_2}} \cdot \frac{V_p}{V_{\mathrm{tot}}} \quad (18)$$

When seeding the jet with 0.001% by volume[1] of TiO_2 particles ($\rho_{\mathrm{TiO_2}} = 4200\,\mathrm{kg/m^3}$) the effective density of the jet changes by 20% with respect to that of pure air. With respect to the effective diameter this results in an increase of 10% over the geometrical diameter, which must be considered when comparing to theory or other data.

EXPERIMENTAL SETUP AND PROCEDURES

Laser and camera setup

The experimental setup is sketched in Figure 2. The rig was composed of existing parts from a generic burner used in our laboratory. In particular a 16mm diameter lance with a length of 150mm having an inner bore of 7.5mm diameter was fixed concentrically in a convergent nozzle of 40mm diameter, which was mounted on a plenum chamber and was used for the reference experiment as described below. Both jet and reference experiment did not use coflow and took place in an environment of air.

For the turbulent jet experiment the 7.5mm bore was connected to a seeding generator fed by metered pressurized air with a flowrate of 80..100 l/min resulting in a jet Reynoldsnumber of $Re = 12\,000$ and a turbulence Reynoldsnumber of $Re_t = 480$. The seeding generator provides titanium dioxide (TiO_2) particles whose size distribution can be approximated by a lognormal distribution with a mean value of $0.4\mu m$ and a standard deviation of $0.3\mu m$. The seeded jet flow forming downstream of the bore exit was illuminated by a PIV laser light sheet in the meridional plane of the jet, while the PIV camera registered the scattered light normal to this plane. In Figure 3 a raw picture of the seeded jet is shown.

The light sheet was oriented at 90 degrees to the flow direction, cutting across from right to left. A commercial High Speed PIV system with a frame rate of 2kHz and $15\mu s$ time separation between laser pulses was used to acquire 2048 double frames having a size of 512x1024 pixels corresponding with a field of view of about 90x180mm. This gives a nominal resolution of 0.176 mm/pix. The field of view was calibrated using a reference target positioned in the measurement plane.

Influence of particle size

As the seeding consists of particles of different size, two effects should be pointed out: First, scattering intensity depends on particle size. This fact, however, is automatically considered by recording seeding PDFs which reflect not only the seeding density and its variation but also the particle size distribution of the seeding. Second, in order to get reliable quantitative data, the seeding particles must be small enough to follow the jet flow. As typical criterion we use the Stokes number St, which is here given by $St = (d_p^2 \cdot \omega \cdot \rho_p)/(18 \cdot \nu \cdot \rho_\infty)$ where d_p denotes the particle diameter, ω the angular frequency of turbulence, ρ_p the density of the particles, ρ_∞ the density of air and ν the kinematic viscosity of air. For $St < 0.32$, particles follow the jet by more than 95%. A rough estimation shows that near the nozzle where the highest velocity gradients can be found all particles with $d_p < 2\mu m$ satisfy this condition. With the above mentioned particle density distribution one obtains that at least 95% of the particles are smaller than $2\mu m$ and are therefore able to follow the fluid without markable delay, whereas downstream this portion becomes even higher because of smaller velocity gradients.

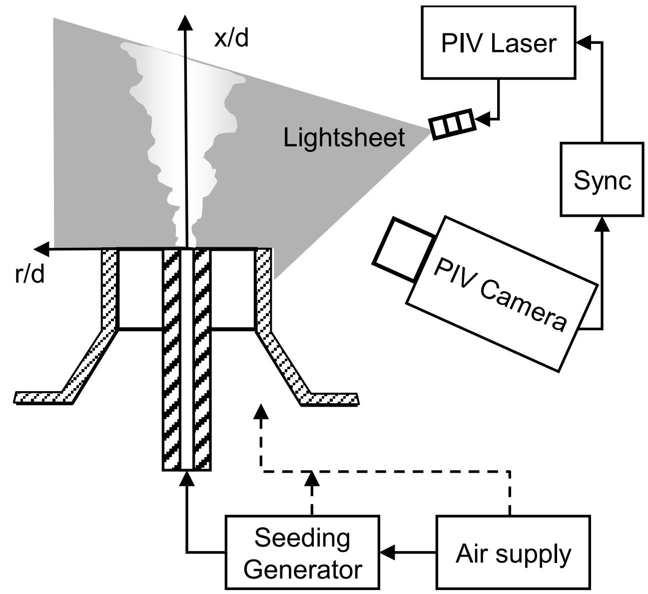

Figure 2. Schematic of the experiment

Camera calibration

The intensity calibration of the HS-CCD camera was checked after some deviation of the measured data from the expected behavior was observed which could only be plausibly explained this way. The calibration curve was obtained placing a LED supplied with constant current in front of the camera and adjusting the shutter timing as to vary the number of photons collected. The top graph in Figure 4 shows the result plotting the camera count over the normalized true photon count. It shows that assuming linearity in particular the lower photon counts will be recorded too high. Contacting the manufacturer on this surprising result it turned out, that this gamma curve is actually built into the camera to reproduce a standardized behavior and could have been switched off. From our experience it is thus advisable to determine the camera calibration anyway.

[1] This gives a high initial number density of $10^4\,1/\mathrm{mm}^3$, however with mixing that drops quickly to $10^3\,1/\mathrm{mm}^3$.

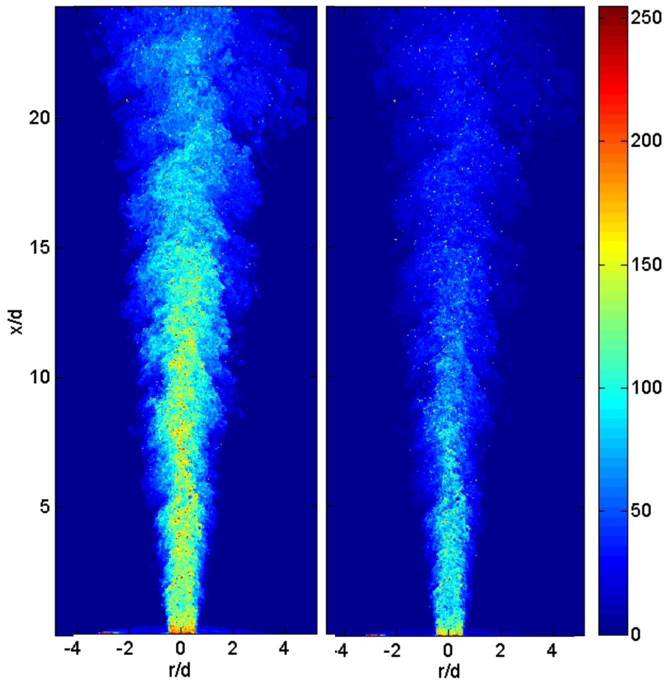

Figure 3. Left: Raw single shot picture of the seeded jet. Colors correspond to camera counts. Right: Single shot picture of the seeded jet after intensity corrections.

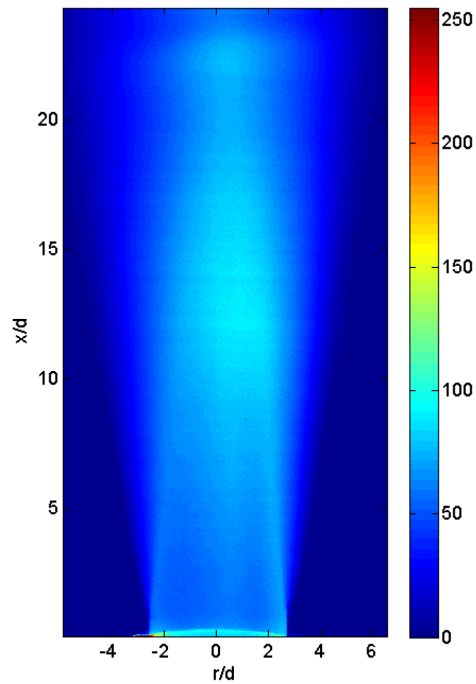

Figure 5. Time average picture of the 40mm nozzle jet.

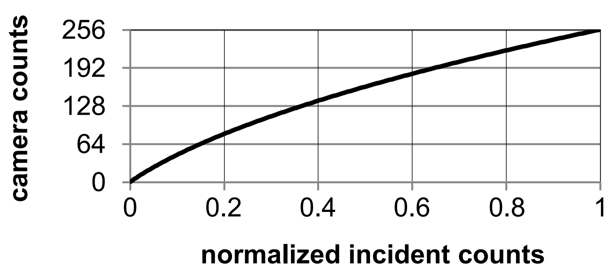

Figure 4. Top: Camera calibration curve showing actual photon count over camera count. Bottom: Fluctuation of total laser power over frame number.

Laser fluctuation

Though intensity fluctuations of the laser illumination are considered when using the proposed PDF method they were investigated to estimate their magnitude. The assessment was based on the consideration that given a huge number of particles in every picture at every instant, summing the pixel intensities in each picture would be indicative of the total laser light intensity. Analyzing the fluctuation of total intensity over 2048 frames we found that there is already a 5% fluctuation in the laser light intensity which would add to the desired turbulence statistics if not considered.

Intensity correction

Since the scattered light intensity depends not only on the particle size and particle density but also on the intensity distribution of the incident light sheet, the latter needs to be factored out of the pictures to obtain quantitative data. Unless a particular setup is used (e.g. [10]) to ensure homogeneous illumination, a calibration experiment is needed to obtain in particular the lateral (i.e. normal to the laser direction) intensity distribution of the light sheet. In this work the light sheet distribution was obtained by feeding seeded flow through the 40mm nozzle. Like this, the region of interest of the 7.5mm nozzle jet experiment is within the core distance of the 40mm nozzle jet. Figure 5 shows the average intensity distribution obtained in the calibration experiment. As the laser intensity does not vary perpendicular to the jet axis, only the intensity distribution on the jet axis is of interest. In Figure 6 the mean intensity variation on the jet axis of the small and big nozzle experiment is plotted over the normalized axial distance. For the small and big jet a peak resulting from reflections is seen at the nozzle. For the big nozzle the intensity has a maximum around $12d$ and a secondary maximum around $22d$. For the small nozzle the intensity is seen to increase with distance before falling off as expected, but for the bump around $22d$. Using the big nozzle distribution the raw intensities in the pictures of the small nozzle jet experiment were corrected in the axial direction as shown for the single shot in Figure 3.

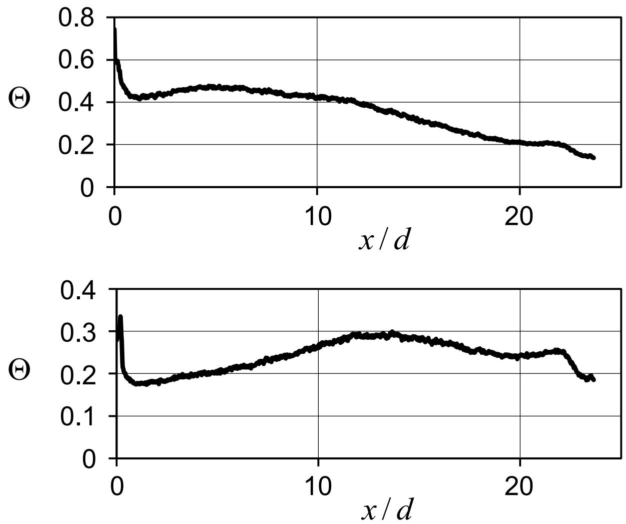

Figure 6. Top: Uncorrected mean intensity distribution on the jet axis from the 7.5mm nozzle experiment. Bottom: Mean intensity distribution on the jet axis from the 40mm nozzle experiment.

Particle rescattering

Becker et al. [8] analysed the effect of optical attenuation by rescattering of the scattered light. They conclude that the effect of attenuation in the camera viewing direction should be negligible, if the attenuation of the light in beam direction is small. Considering the radial profiles of mean mixture fraction shown in Figure 10 the almost perfect symmetry to the maximum radial coordinate[2], indicates that particle density was low enough such that the attenuation in the beam direction is negligible.

PDF measurement

As a PDF is a statistical function, a large number of samples is necessary for good data convergence. Considering that our PIV run consisted of 2048 picture pairs sampling only one pixel per picture for a given location will not be sufficient as there are 256 bins to be filled. Since the large turbulence scales are much bigger than a pixel, it is allowable to use a number of pixels to represent a location. We found that a 13x9 pixel region would work very well, giving about 240000 samples per run at a resolution of the order of millimeters if no overlap is allowed. Referring to the definition in eqn. 3 we place one of these regions close to the nozzle outlet into the core region of the jet to obtain $p_\omega = p_\Theta(f = 1)$.

Experimental procedure

As described above, the experiment had to be performed twice using two different nozzle diameters, in order to provide data for the intensity correction procedure.

In the first part of the experiment, the 7.5mm nozzle was connected to the seeding generator and a series of 2048 image pairs was recorded, using the PIV setup which has already been described in detail. Thereby the seeding density had to be chosen higher than for PIV experiments because here not only single particle movement but also particle density variations are of interest. As the recorded light intensity of first and second shot of an image pair usually differ, only one image per pair could be used in the following. In order to reduce computing time, PDFs were not created for each of the 512x1024 pixels but only for 21x41 grid points which covered the area of interest. Generating PDFs from the image series one has to consider the nonlinearity of the camera which means that the camera counts of each pixel have to be converted into intensity values using the camera calibration curve.

For the reference experiment, the 7.5mm nozzle had to be removed from the rig, instead the 40mm nozzle was connected to the seeding generator. Due to the higher flowrate through the big nozzle the seeding/air ratio had to be adjusted so that the seeding density was low enough to exclude particle rescattering.

As already mentioned only reference PDFs of grid points on the jet axis are needed for the intensity correction. The mean values of these PDFs determine the factor by which the jet PDFs have to be stretched in order to correct the variation of the laser intensity along the jet axis.

Finally, the local mixture fraction PDF p_f was calculated from p_Θ and p_ω for each grid point using the numerical inversion procedure described above.

RESULTS

Comparison of inversion methods

Figure 7 gives the comparison of PDFs obtained downstream on the jet axis using the numerical method (thick line) and the analytical inversion (thin line). In this location the PDFs are expected to be Gaussian. Therefore the analytical inversion oscillates fairly little and the comparison between both distributions is good. Nevertheless, it can be seen that the low pass filter used in the analytical inversion process broadens the PDF compared to the one obtained by numerical inversion. Therefore, for all further calculations the latter method was used.

Fields of mean and variance

Figure 8 and 9 give an overview of the data that can be obtained using the proposed method. The mean value distribution in Figure 8 shows the expected transition from a top hat to a Gaussian profile with the associated jet spreading which is accompanied by the hyperbolical decrease of the centerline values with increasing distance. Here we may note that the mean value distribution obtained from direct time average of the corrected pictures is, within a deviation of less than 0.5%, identical to that of the PDF

[2] The jet was not perfectly aligned with the coordinate axis by about $0.002d$.

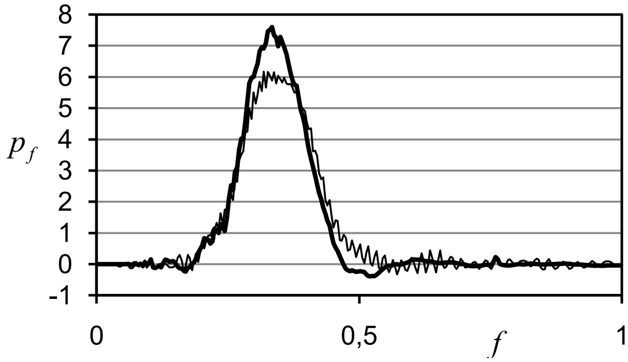

Figure 7. Comparison of mixture fraction PDF from analytical solution (thin line) and numerical solution ($(x-x_0)/d = 20$, $Re = 12000$).

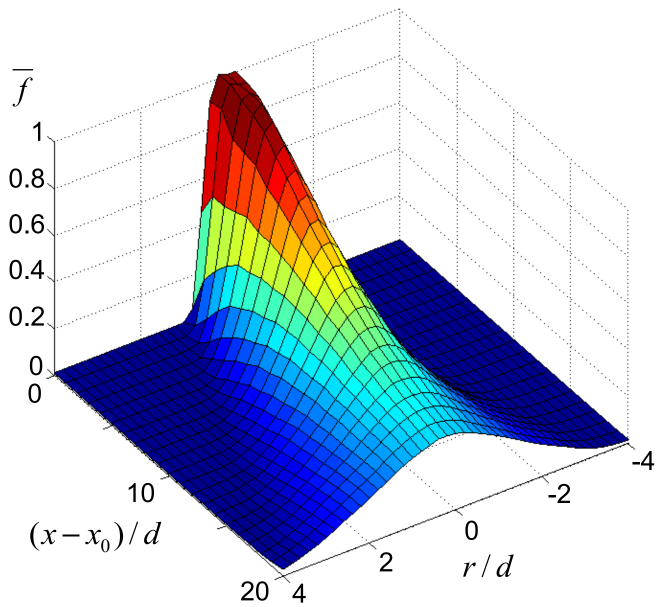

Figure 8. Field of mean mixture fraction in the current experiment ($Re = 12000$).

method. This indicates that the regularization procedure is robust. The mixture fraction variance seen in Figure 9 shows a double maximum with high values of variance close to the nozzle which is associated with the steep velocity and mixing gradients that form on either side of the jet core region. As the jet spreads the gradients decrease and with them the production of fluctuations diminishes too. In Figure 10 radial profiles of mean and RMS of mixture fraction are shown at three axial stations $x/d = 14, 17, 20$. These have been normalized with the respective mean value on the jet centerline f_c. As expected from self similarity the profiles collapse very well. Close to the center of the jet the profiles of the RMS do not match. In particular a decrease

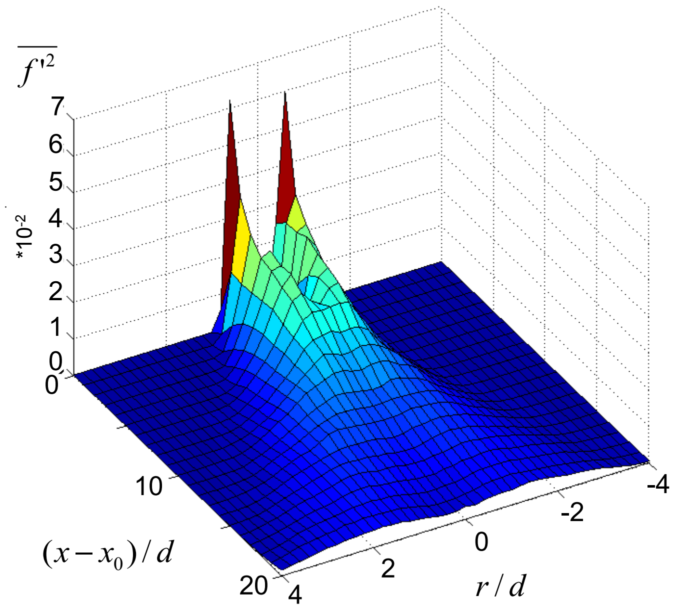

Figure 9. Field of mixture fraction variance in the current experiment ($Re = 12000$).

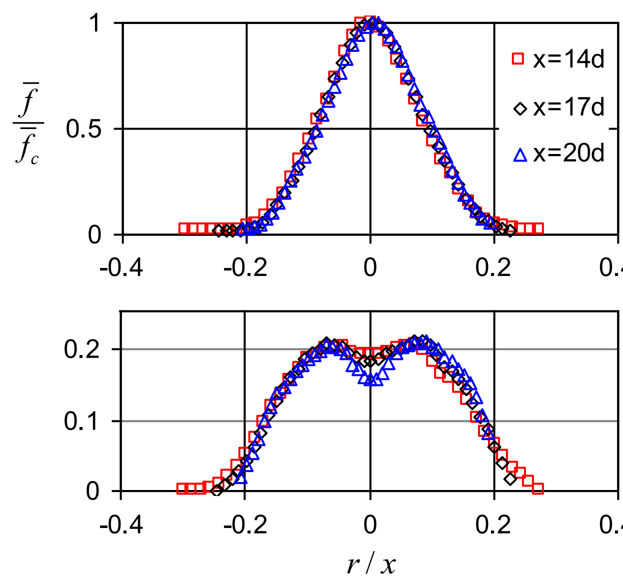

Figure 10. Radial profiles of normalized mean and RMS value of mixture fraction in the current experiment ($Re = 12000$).

is observed with increasing nozzle distance. This indicates that also the RMS profile is converging towards a self similar profile that is governed only by production on the shear layer, whereas further upstream still the influence of the transition from core to similarity region is felt.

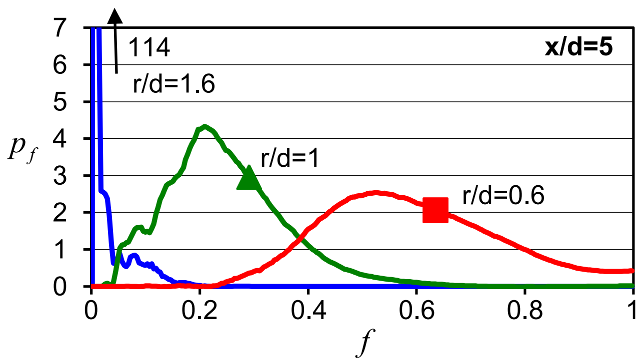

Figure 11. PDF of mixture fraction in the near field of the jet ($(x-x_0)/d=5$, $Re=12000$) at the radial location $r/d=0.6$ (square), $r/d=1.0$ (triangle) and $r/d=1.6$ (plain line).

PDF resolution in the near field

To demonstrate the capability of the method PDF data was taken in three radial locations $r/d=0.6, 1.0, 1.6$ in the transition zone at $x/d=5$ between core and similarity region. The result, which is plotted in Figure 11, complies with our expectation to see a transition from Gaussian to clipped Gaussian behavior towards the jet edge due to intermittence. It is interesting to note, that even for $r/d=1.6$ where large intermittence is present, a small mixed region is indicated by the PDF.

Validation

The turbulent round jet theory being well established, we first compare our mean value data with theory in Figure 12. There the circles give the data as obtained from our experiment and the solid lines show the theory from eqn. 16. The comparison is very good. To obtain the jet density ρ_0 eqn. 18 was used, estimating the volume fraction of the particles from the average seeding consumption typical in our lab. This gives a density ratio of 1.16 which makes a 7% correction of the experimental jet diameter necessary in comparison with theory and other data. In the typical PIV experiment normally the seeding density is stepped down by at least a factor 10 by mixing the seeding generator flow into the experimental flow that has a much higher mass flow rate, so the seeding density influence may be neglected. The problem is typical of tracer concentration measurements: On one side much tracer is desirable to get high signal also at low mixture fraction. On the other side the influence of seeding may distort the result.
To validate the quality of the PDF measurement, the radial and axial profiles of the RMS values are compared with literature in Figures 13. In the top graph the radial profile of the RMS value normalized with the centerline mean value (solid line) is compared with the data from Dowling and Dimotakis [1]. While the general shape of the profiles agrees well, there is a constant offset of about 5%. Since our RMS measurements shown in Figure 10 show little dependence of the axial station they should be

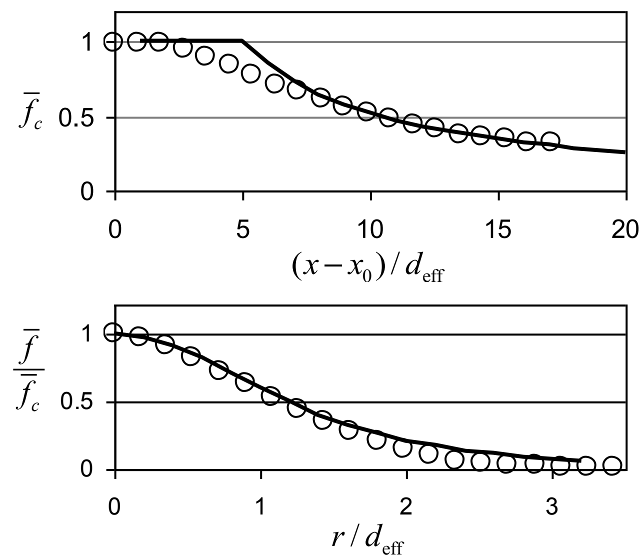

Figure 12. Top: Normalized axial profile at $r/d=0$ (circles, $Re=12000$) from this work and theory (eqn. 16, line). Bottom: Normalized radial profile at $x/d=10$ (circles, $Re=12000$) from this work and theory (eqn. 16, line).

well comparable with the reference though the axial stations are not identical. Therefore comparison was sought with a different source (Corrsin and Uberoi cited in [11]) which is shown on the bottom plot of Figure 13. Here the values along the jet axis are given, which agree very well in the similarity range. Knowing that the laser power fluctuation in our experiment is in the order of 5% we can only speculate that maybe this temporal fluctuation has not been accounted for in [1].
Finally in Figure 14 we compare the shape of the PDF at $(x-x_0)/d=20$ and $r/d=2.5$ as determined here with that of [1]. While differences of 10-20% are seen locally, the shape of the PDFs in this intermittent region with local minima and maxima compares very well.

SUMMARY AND CONCLUSIONS

In this paper a new method is presented to obtain mixture fraction statistics from planar images of particle seeded flow in terms of probability density functions (PDF). Introducing a model for the PDF of the observed scattered light that connects this with the PDF of seeding density and mixture fraction, we give an analytical and a numerical inversion procedure to extract the mixture fraction PDF from the measured PDFs of scattered light and particle density. We demonstrate the technique on the example of a turbulent round free jet, explaining in detail the steps taken to obtain the data. Finally we show measured data and compare with theory and literature. From the comparison we can draw the following conclusions.

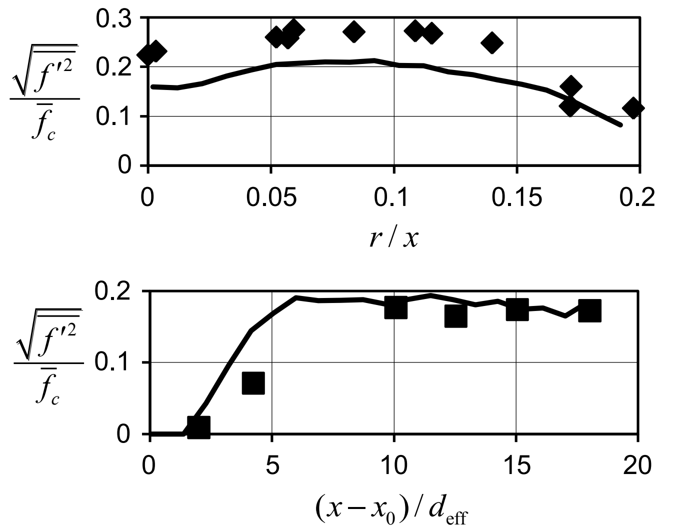

Figure 13. Top: Normalized radial RMS profiles at $(x-x_0)/d_{\mathrm{eff}} = 17.3$ from this work (line, $Re = 12000$) and literature (diamonds, $(x-x_0)/d = 20$, $Re = 5000$, from [1]). Bottom: Normalized axial RMS profiles on axis from this work (line, $Re = 12000$) and literature (squares, $Re = 20000$, from [11]).

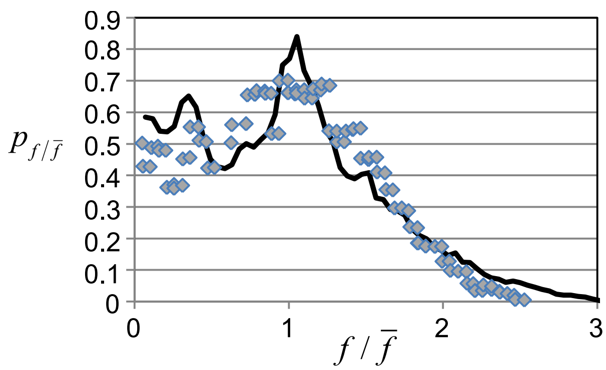

Figure 14. PDF of normalized mixture fraction 7° off the jet centerline at $(x-x_0)/d = 20$ from this work (line, $Re = 12000$) and literature (Symbols, from [1]).

1. The new method is capable of measuring planar field statistics of mixture fraction using PIV particle seeded flow and standard PIV equipment.
2. The comparison with theory and other data is very favorable, indicating that quantitative measurements can be made.
3. With this method a practicable tool for combustor design mixing studies has been developed, which could find broad application as it uses PIV equipment that has entered combustion labs already.

While our results are very encouraging further work is needed to prove the method in situations with density gradient and combustion. As sketched above, the basic approach is already clear for density gradients in non-reacting mixtures. For combustion situations we also see a promising procedure, but the relevant experiments are by far more involved than the current study and will be reported later.

ACKNOWLEDGMENT

This project was supported by Alstom, Bayerische Forschungsstiftung, Bayerisches Staatsministerium für Wirtschaft, Forschung und Kunst and Bayerisches Staatsministerium für Wirtschaft, Infrastruktur und Technologie in the framework of KW21 which is gratefully acknowledged.

REFERENCES

[1] Dowling, D., and Dimotakis, P., 1990. "Similarity of the concentration field of gas phase turbulent jets". *J. Fluid Mech.*, **218**, pp. 109–141.

[2] Bergmann, V., Meier, W., Wolff, D., and Stricker, W., 1998. "Application of spontaneous raman and rayleigh scattering and 2d lif for the characterization of a turbulent ch4/h2/n2 jet diffusion flame.". *Appl. Phys.*, **B 66**, pp. 489–502.

[3] King, G., Dutton, J., and Lucht, R., 1999. "Instantaneous, quantitative measurements of molecular mixing in the axisymmetric jet near field". *Phys. Fluids,* **11, No.2**, pp. 403–416.

[4] Rosensweig, R., Hottel, H., and Williams, G., 1961. "Smoke-scattered light measurements of turbulent concentration fluctuations". *Chem. Engr. Science,* **15, Issue 1-2**, pp. 111–129.

[5] Becker, H., Hottel, H., and Williams, G., 1967. "The nozzle fluid concentration field in the turbiulent round free jet". *J. Fluid Mech.,* **30 part 2**, pp. 259–284.

[6] Shaughnessy, E., and Morton, J., 1977. "Laser light-scattering measurements of particle concentration in a turbulent jet". *J. Fluid Mech.,* **80, part 1**, pp. 129–148.

[7] Sautet, J., and Stepowski, D., 1994. "Single-shot laser mie scattering measruements of the scalar profiles in the near field of turbulent jets with variable densities". *Experiments in Fluids,* **16**, pp. 353–367.

[8] Becker, H., Hottel, H., and Williams, G., 1967. "On the light-scatter technique for the study of turbulence and mixing". *J. Fluid Mech.,* **30 part 2**, pp. 259–284.

[9] Hansen, P., and O'Leary, D., 1993. "The use of the l-curve in the regularization of discrete ill-posed problems". *SIAM J. Sci. Comput.,* **Vol. 14 No. 6**, pp. 1487–1503.

[10] Pfadler, S., Beyrau, F., Löffler, M., and Leipertz, A., 2006. "Application of a beam homogenizer to planar laser diagnostics". *OPTICS EXPRESS,* **Vol.14, No.22**, pp. 10171–10180.

[11] Hinze, J. O., 1959. *Turbulence*, 2nd edition ed. Mc Graw-Hill. ISBN 0-07-029037-7.